Electronic Supplementary Material (ESI) for Inorganic Chemistry Frontiers.

Supporting Information

A Binuclear Copper Center-Incorporated Photocatalyst Applied in Mimicing Enzyme Catalysis for Aerobic Hydroxylation of Phenylboronic Acids

Chen Si[a], Xueling Liu[a], Junjie Xu[a], Jiangbo Xu[a], Pengtao Ma[a], Qiuxia Han[a,*]

Henan Key Laboratory of Polyoxometalate Chemistry, College of Chemistry and Molecular Sciences, Henan University, Kaifeng, Henan 475004, P. R. China

*Corresponding author. E-mail address: hdhqx@henu.edu.cn

Contents

1. Supplementary Materials and Methods

All solvents and reagents obtained from commercial sources were used without further purification. The Dawson-type polyoxometalate $K_{12}[\alpha\text{-}H_2P_2W_{12}O_{48}]_{24}\cdot H_2O$ was prepared according to the literature and characterized by IR spectroscopy.[s1] The EA of C, H and N were recorded on a Vario EL III elemental analyzer of the Flash 2000 analyzer and Optima 2100 DV. Fourier-transform infrared (FTIR) spectra of samples were recorded in a JASCO FT/IR-430 spectrometer over a range of 4000–400 cm^{-1}. The UV-vis diffuse reflectance spectra (DRS) were obtained on a HITACHI U-4100 UV-ViseNIR spectrometer equipped with 60 mm diameter integrating sphere using finely ground sample, at room temperature. The powder X-ray diffraction (PXRD) spectra were recorded on a Rigaku Model D/Max-2400 X-ray diffractometer with a sealed copper tube (λ = 1.54178 Å) in the angular range 2θ = 5–50°. Water contents were determined by TG analyses on a Mettler-Toledo TGA/SDTA 851^e instrument with a heating rate of 10 °C min^{-1} heated from 25 to 800 °C under nitrogen. Inductively Coupled Plasma (ICP) of Cu, B, and W analyses were performed on a Jarrel-AshJ-A1100 spectrometer. The photocatalytic reaction was performed on WATTCAS Parallel Light Reactor (WP-TEC-1020HSL) with 10W 6000-6500K white COB LED. Photocurrent measurements were conducted on a CHI 660E electrochemical workstation (Shanghai Chenhua Instrument Co., China) in a standard three-electrode system. The Ag/AgCl electrode and platinum foil were used as the reference electrode and counter electrode, respectively. Furthermore, the 25 mg catalyst was dispersed uniformly in 1 mL (H_2O/Et_2OH=1/4) solution by ultrasound. The 80 uL above solution was coated on an indium tin oxide (ITO) glass (2 cm×1 cm) to dry naturally. Finally, the sample was covered with 40ul solution (Nafion: Et_2OH = 1:3). In the frequency range from 0.1 to 100 000 Hz, the electrochemical impedance spectra (EIS) data were collected. The visible light source was a 300 W Xe lamp. The yields were tested on a gas chromatograph (Agilent 8860G2790A). The photoluminescence (PL) properties were obtained on a EDINBURGH FLS 980 fluorescence spectrophotometer equipped, which have a 450 W xenon lamp.

2. Single-crystal X-ray Crystallography

A good single crystal of **Cu(I)W–TPT** with dimensions of 0.1 × 0.08 × 0.12 mm^3 was prudentially picked under an optical microscope and sealed to a glass tube closed at both ends. A suitable crystal was selected and on a Bruker D8 VENTURE PHOTON II diffractometer with graphite-monochromated Mo Kα (λ = 0.71073 Å) at 284(2) K using SAINT and SMART programs. The crystal was kept at 168.08 K during data collection. Using Olex2[s2], the structure was solved with the olex2.solve[s3] structure solution program using Charge Flipping and refined with the ShelXL[s4] refinement package using Least Squares minimisation. All the atoms were refined anisotropically in the last refinement cycle. H atoms were fixed in calculated positions and then refined using a riding model. All of them are directly included in the molecular formula. The CCDC number of **Cu(I)W–TPT** is 2280692. Crystallographic data and structure refinements for **Cu(I)W–TPT** are listed in Table S1.

Table S1. Crystal data and structure refinement for **Cu(I)W–TPT**.

Crystal data	**Cu(I)W–TPT**
empirical formula	$C_{54}H_{36}Cl_{0.5}Cu_2N_{18}O_{69.5}P_2W_{18}$
crystal system	triclinic
space group	P-1
a (Å)	14.1811(16)
b (Å)	17.970(3)
c (Å)	20.978(2)
α (deg)	91.429(6)
β (deg)	92.792(3)
γ (deg)	99.305(6)
V (Å^3)	5266.5(12)
Z	2
T, K	168.08
μ / mm^{-1}	20.111
F(000)	4941.0
2ϑ (deg)	4.34 - 50.2
Index ranges	−16 ≤ h ≤ 16, −21 ≤ k ≤ 21, −24 ≤ l ≤ 25
Reflections collected / unique	66019 / 18720 [Rint = 0.0410, Rsigma = 0.0409]
Data / restraints / parameters	18720 / 6 / 1465
GOF	1.024
R_1[a] [(I > 2*s*(I))]	0.0344
wR_2[b] [I > 2*s*(I)]	0.0818
R_1[a] (all data)	0.0442
wR_2[b] (all data)	0.0863
diff peak and hole, eÅ^{-3}	2.04 / -2.53

[a] $R_1 = \sum||Fo| - |Fc||/\sum|Fo|$, [b] $wR_2 = [\sum w(Fo^2 - Fc^2)^2/\sum w(Fo^2)^2]^{1/2}$; w = 1/[σ^2(Fo^2) + (xP)^2 + yP], P= (Fo^2 + 2Fc^2)/3, where x = 0.0315, y = 65.1509 for **Cu(I)W–TPT**.

Table S2. The selected bond lengths and angles of **Cu(I)W–TPT**.

Bond	Length	Bond	Length
W(1)–O(5)	1.865(7)	W(14)–O(30)	1.903(8)
W(1)–O(9)	1.854(7)	W(15)–O(10)	1.902(8)
W(2)–O(6)	1.909(7)	W(15)–O(17)	1.920(7)
W(2)–O(19)	2.366(7)	W(16)–O(4)	2.340(7)
W(3)–O(27)	1.956(7)	W(16)–O(11)	1.927(7)
W(3)–O(35)	1.877(7)	W(17)–O(1)	2.442(7)
W(4)–O(13)	1.880(7)	W(17)–O(7)	1.910(7)
W(4)–O(12)	1.958(7)	W(18)–O(2)	2.378(7)
W(5)–O(2)	2.329(6)	W(18)–O(13)	1.941(7)
W(5)–O(9)	1.999(7)	P(00L)–O(2)	1.526(7)
W(6)–O(1)	2.257(6)	P(00L)–O(4)	1.528(7)
W(6)–O(7)	1.893(7)	P(00L)–O(19)	1.532(7)
W(7)–O(30)	1.934(8)	P(00L)–O(43)	1.579(7)
W(7)–O(31)	1.871(7)	P(00M)–O(1)	1.540(7)
W(8)–O(3)	2.373(7)	P(00M)–O(3)	1.534(7)
W(8)–O(6)	1.896(7)	P(00M)–O(37)	1.529(7)
W(9)–O(4)	2.398(7)	P(00M)–O(61)	1.581(7)
W(9)–O(5)	2.008(7)	Cu(1)–N(3)	2.016(9)
W(10)–O(3)	2.339(7)	Cu(1)–N(7)	2.021(9)
W(10)–O(8)	1.894(7)	Cu(1)–O(44)	1.959(7)
W(11)–O(23)	1.870(7)	Cu(1)–O(2W)	1.969(8)
W(11)–O(34)	1.931(8)	Cu(1)–O(1W)	2.383(9)
W(12)–O(12)	1.902(7)	Cu(2)–N(9)	2.004(8)
W(12)–O(17)	1.906(7)	Cu(2)–N(13)	2.012(9)
W(13)–O(8)	1.881(7)	Cu(2)–O(48)[1]	2.348(7)
W(13)–O(19)	2.393(6)	Cu(2)–O(3W)	2.024(8)
W(14)–O(22)	1.909(7)	Cu(2)–O(4W)	1.9316(13)

Bond	Angle	Bond	Angle
O(5)–W(1)–O(14)	88.3(3)	O(13)–W(18)–O(2)	84.4(3)
O(5)–W(1)–O(36)	158.9(3)	O(13)–W(18)–O(27)	166.6(3)
O(6)–W(2)–O(19)	83.2(3)	O(2)–P(00L)–O(4)	111.4(4)
O(6)–W(2)–O(29)	89.6(3)	O(2)–P(00L)–O(19)	111.0(4)
O(14)–W(3)–O(43)	72.8(3)	O(2)–P(00L)–O(43)	107.0(4)
O(28)–W(3)–O(14)	157.7(3)	O(4)–P(00L)–O(19)	112.4(4)
O(13)–W(4)–O(32)	157.2(3)	O(4)–P(00L)–O(43)	107.9(4)
O(13)–W(4)–O(36)	88.9(3)	O(19)–P(00L)–O(43)	106.9(4)
O(9)–W(5)–O(2)	80.8(3)	O(1)–P(00M)–O(61)	107.1(4)
O(15)–W(5)–O(2)	74.0(3)	O(3)–P(00M)–O(0)	111.4(4)
O(7)–W(6)–O(1)	75.4(3)	O(3)–P(00M)–O(61)	107.6(4)

O(7)−W(6)−O(20)	161.5(3)	O(37)−P(00M)−O(1)	111.3(4)
O(30)−W(7)−O(40)	86.1(3)	O(37)−P(00M)−O(3)	111.7(4)
O(30)−W(7)−O(61)	72.3(3)	O(37)−P(00M)−O(61)	107.4(4)
O(6)−W(8)−O(3)	84.4(3)	N(3)−Cu(1)−N(7)	157.9(4)
O(6)−W(8)−O(16)	90.9(3)	N(3)−Cu(1)−O(1W)	97.1(4)
O(5)−W(9)−O(4)	80.7(3)	N(7)−Cu(1)−O(1W)	103.9(4)
O(11)−W(9)−O(4)	72.9(3)	O(44)−Cu(1)−N(3)	89.6(3)
O(8)−W(10)−O(3)	82.8(3)	O(44)−Cu(1)−N(7)	86.8(3)
O(8)−W(10)−O(16)	89.4(3)	O(44)−Cu(1)−O(2W)	169.1(3)
O(23)−W(11)−O(34)	89.9(3)	O(44)−Cu(1)−O(1W)	81.4(3)
O(23)−W(11)−O(40)	156.2(3)	O(2W)−Cu(1)−N(3)	93.6(4)
O(12)−W(12)−O(17)	158.3(3)	O(2W)−Cu(1)−N(7)	94.0(4)
O(12)−W(12)−O(24)	88.0(3)	O(2W)−Cu(1)−O(1W)	87.8(3)
O(8)−W(13)−O(19)	82.8(3)	N(9)−Cu(2)−N(13)	170.1(4)
O(8)−W(13)−O(26)	90.0(3)	N(9)−Cu(2)−O(48)^{1}	97.3(3)
O(22)−W(14)−O(34)	157.8(3)	N(9)−Cu(2)−O(3W)	89.1(3)
O(22)−W(14)−O(39)	85.3(3)	N(13)−Cu(2)−O(48)^{1}	92.5(3)
O(10)−W(15)−O(17)	157.0(3)	N(13)−Cu(2)−O(3W)	93.3(3)
O(10)−W(15)−O(23)	84.9(3)	O(3W)−Cu(2)−O(48)^{1}	83.3(3)
O(11)−W(16)−O(4)	74.1(3)	O(4W)−Cu(2)−N(9)	87.5(3)
O(11)−W(16)−O(38)	88.9(3)	O(4W)−Cu(2)−N(13)	90.5(3)
O(7)−W(17)−O(1)	70.7(3)	O(4W)−Cu(2)−O(48)^{1}	94.29(19)
O(7)−W(17)−O(22)	90.4(3)	O(4W)−Cu(2)−O(3W)	175.6(2)

3. Additional Structural and Characterizational Figures.

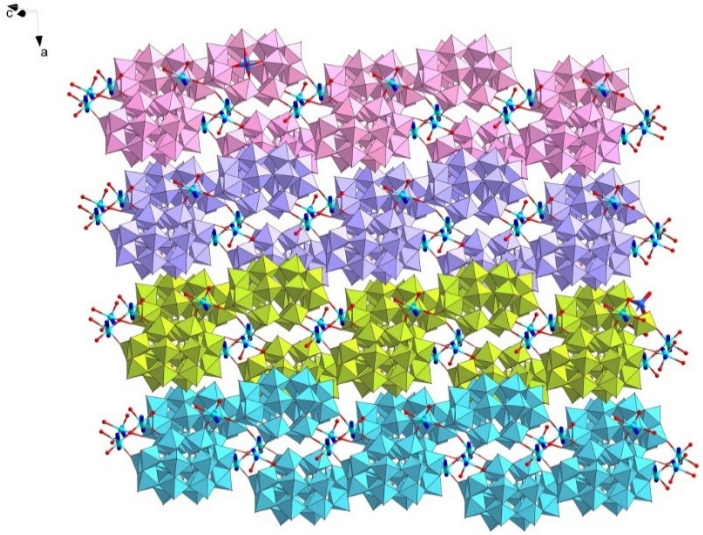

Figure S1. 3D open network of the **Cu(I)W–TPT**.

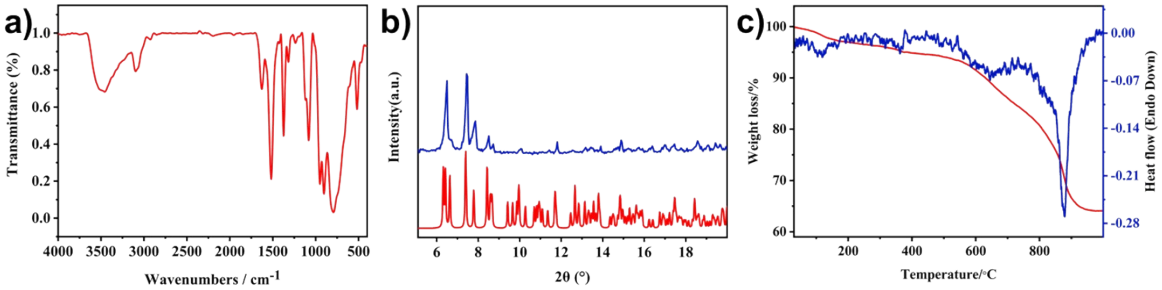

Figure S2. (a) IR spectra; (b)PXRD patterns (bottom, simulated; top, experimental); (c)TG-DTA of **Cu(I)W–TPT**.

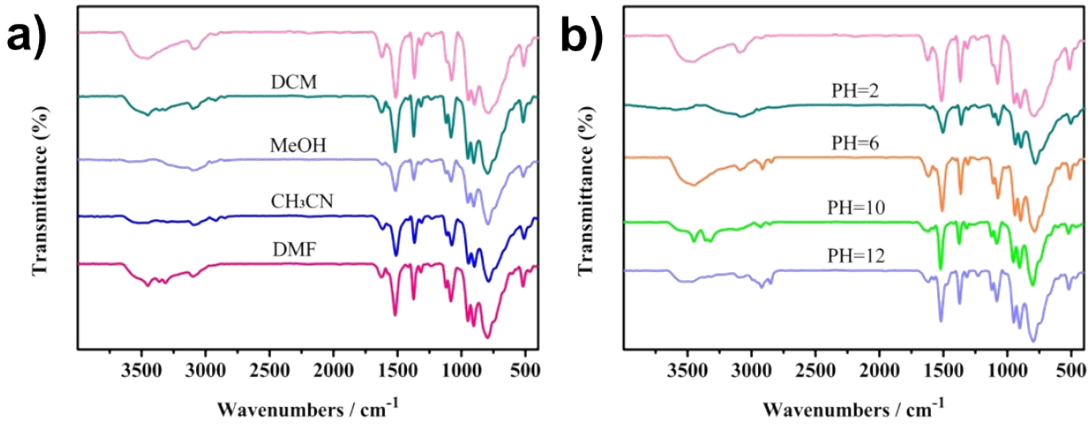

Figure S3. (a) IR spectra of **Cu(I)W–TPT** in different organic solvents. (b) IR spectra of **Cu(I)W–TPT** in different aqueous with different pH values. The pH values were adjusted with 0.5 mol·L^{-1} HCl (pH=2) and NaOH solutions (pH=10,12), respectively.

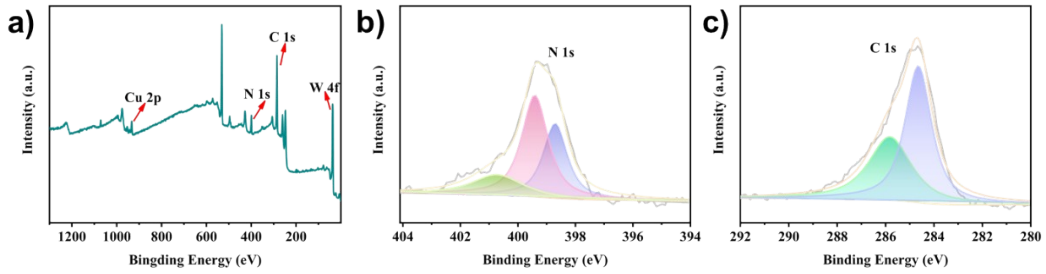

Figure S4. (a) XPS survey spectra of **Cu(I)W–TPT**; (b, c)The high-resolution XPS spectra of N 1s and C 1s.

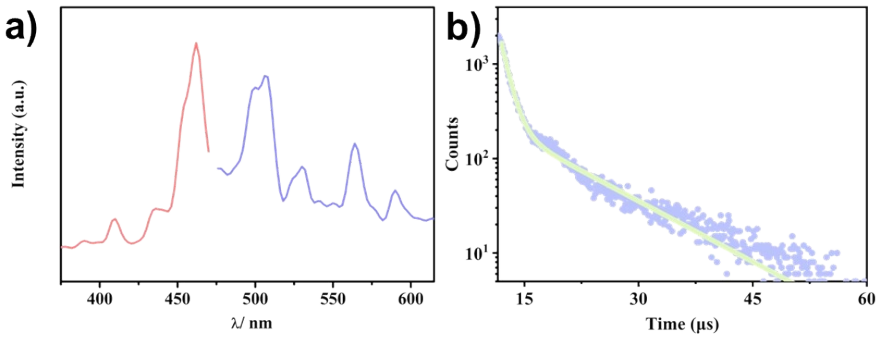

Figure S5. (a, b) Excitation and emission spectra and Luminescence lifetime curve of **Cu(I)W–TPT**.

4. Additional Catalysis Details

The photocatalytic reaction was performed on WATTCAS Parallel Light Reactor with continuous cooling water equipment (WP-TEC-1020HSL). In a typical reaction system, phenylboronic acid (0.5 mmol), catalyst **Cu(I)W–TPT** (10 mg), Et_3N (0.6 mmol), and acetonitrile (2 mL) were added to a quartz tube (15 mL) equipped with a stir bar. A 10 W 6000-6500 K white COB LED was used as the light source by bottom irradiation. The temperature of the reaction was in the range of 25 ± 5 °C. After 24 h of reaction, the mixture was centrifuged to remove **Cu(I)W–TPT** samples. Then, the mixture was extracted with ethyl acetate, dried with anhydrous Na_2SO_4. The product was obtained by rotary evaporation at 40 °C. The conversion and selectivity were determined by ^{1}H NMR.

Figure S6. Sketch portrays the reaction setup.

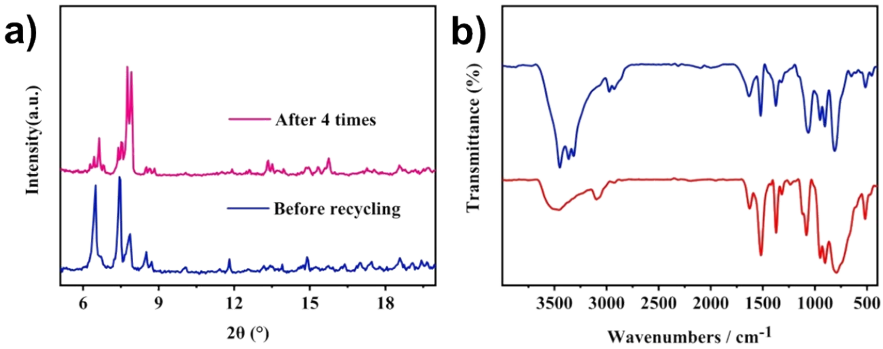

Figure S7. (a, b) FT-IR spectra and PXRD patterns after four recycles of **Cu(I)W–TPT**.

Table S3. Summary of the activity of photocatalytic oxidation of Phenylboronic acid

Catalyst	T(℃)	Light sourse	Oxidant	Additives	t (h)	Yield (%)	Ref.
LZU-190-COF	r.t	20 W white LEDs	air	iPr_2NEt	48	99	S4
Zr-TCPCo	r.t	450 nm LED irradiation	O_2	Et_3N	24	91	S5
CCN-P	r.t	blue LED lamp	O_2	Et_3N	4	99	S6
EFC-CMP	r.t	blue LEDs	air	DIPEA	1.3	91	S7
UiO-67-Ru(bpy)3-MOF	r.t	UV-365	air	iPr_2NEt	48	81	S8
N-C/In_2O_3 HD	r.t	blue LEDs	air	DIPEA	24	99	S9
Cz-POF-1	r.t	Fluorescence lamp	air	Et_3N	24	94	S10
CPOP-29	r.t	white LEDs	air	iPr_2NEt	48	98	S11
This work	r.t	10 W white LEDs	air	Et_3N	24	99	

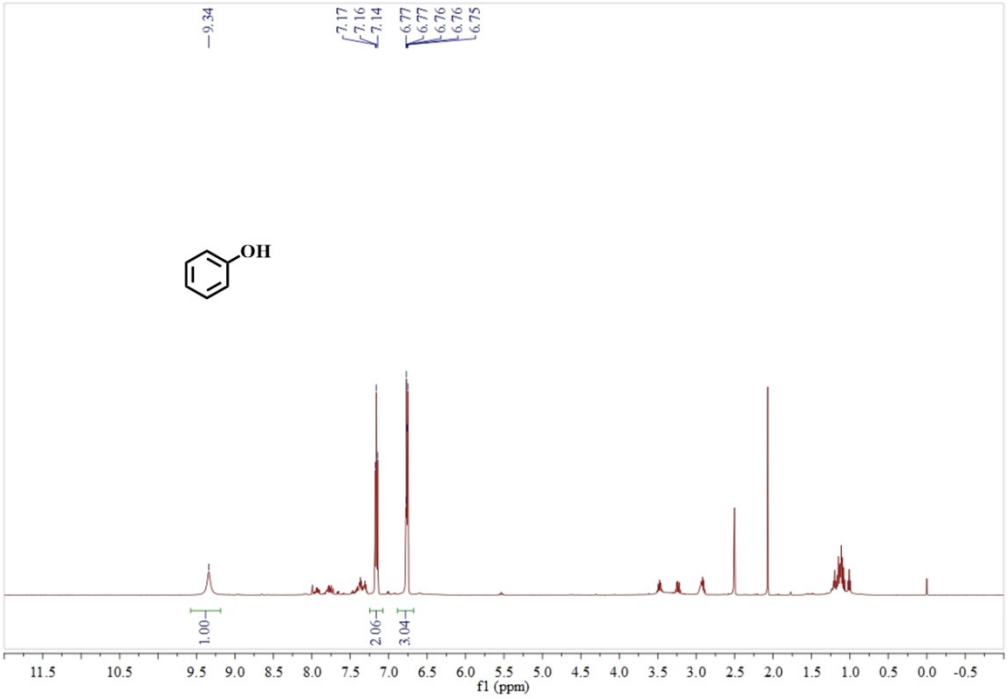

Figure S8. ^{1}H NMR spectrum of phenyl hydroxide

^{1}H NMR (500 MHz, DMSO) δ 9.34 (s, 1H), 7.16 (t, J = 7.9 Hz, 2H), 6.89 – 6.67 (m, 3H).

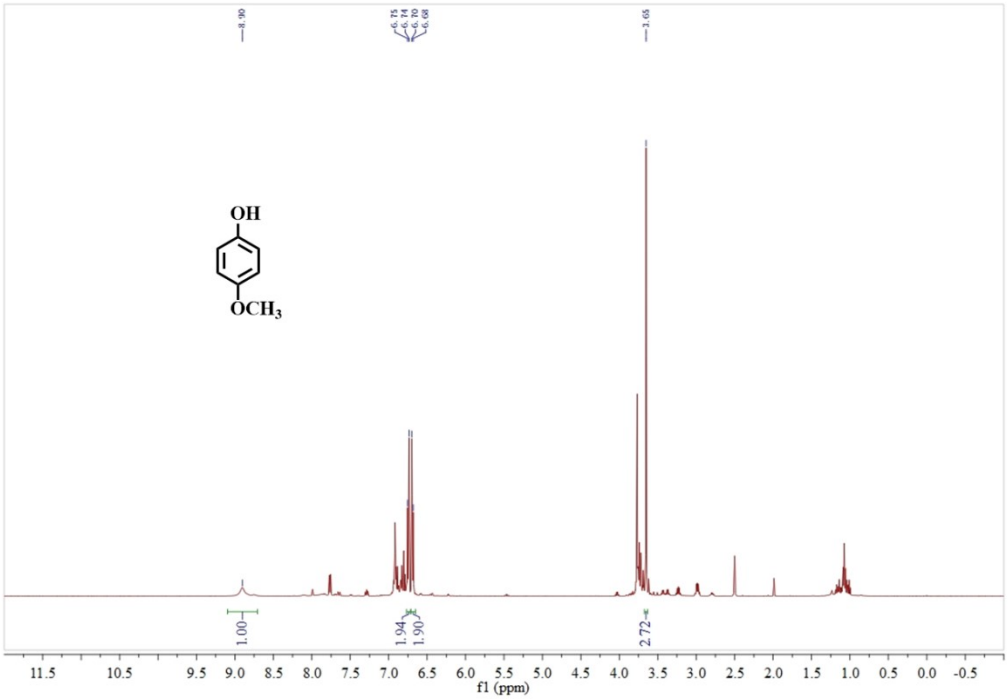

Figure S9. ^{1}H NMR spectrum of 4-Methoxyphenol

^{1}H NMR (500 MHz, DMSO) δ 8.90 (s, 1H), 6.75 (d, J = 9.0 Hz, 2H), 6.69 (d, J = 9.0 Hz, 2H), 3.65 (s, 3H).

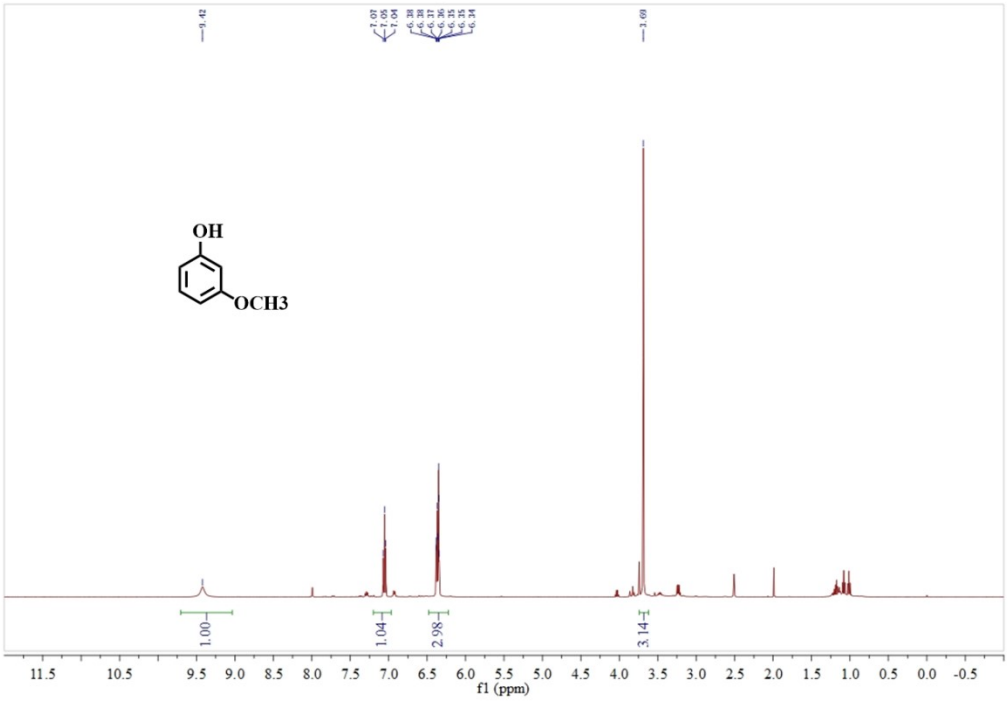

Figure S10. ^{1}H NMR spectrum of m-Methoxyphenol

^{1}H NMR (500 MHz, DMSO) δ 9.42 (s, 1H), 7.05 (t, J = 8.1 Hz, 1H), 6.48 – 6.23 (m, 3H), 3.69 (s, 3H).

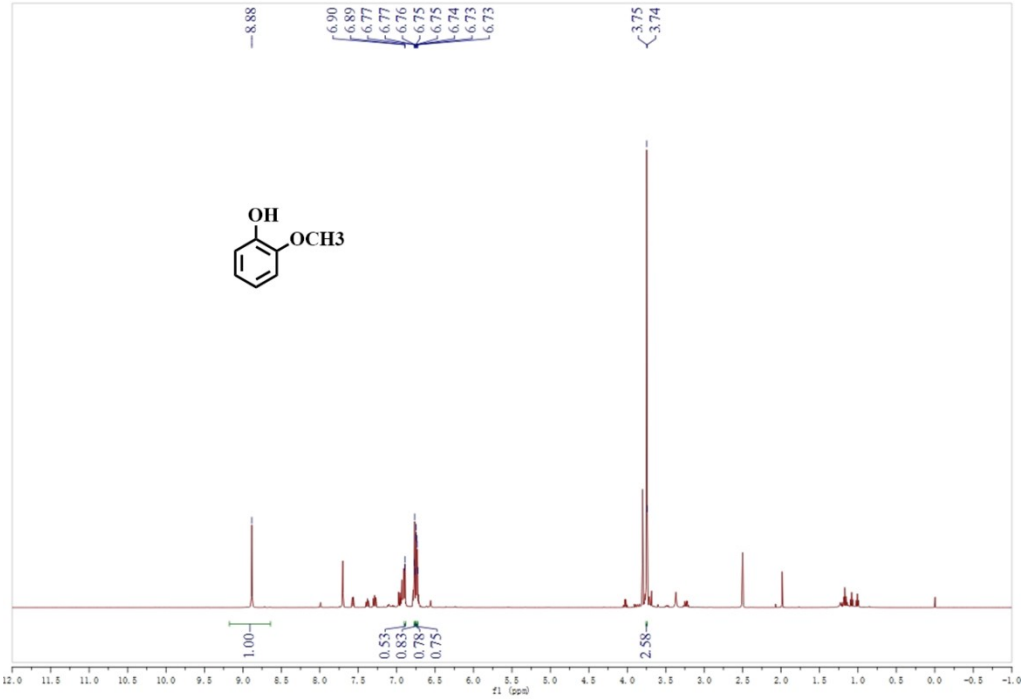

Figure S11. ^{1}H NMR spectrum of 2-methoxy-Phenol

^{1}H NMR (500 MHz, DMSO) δ 8.88 (s, 1H), 6.89 (d, J = 2.6 Hz, 1H), 6.77 (t, J = 2.1 Hz, 1H), 6.75 (d, J = 2.5 Hz, 1H), 6.74 – 6.72 (m, 1H), 3.75 (s, 3H).

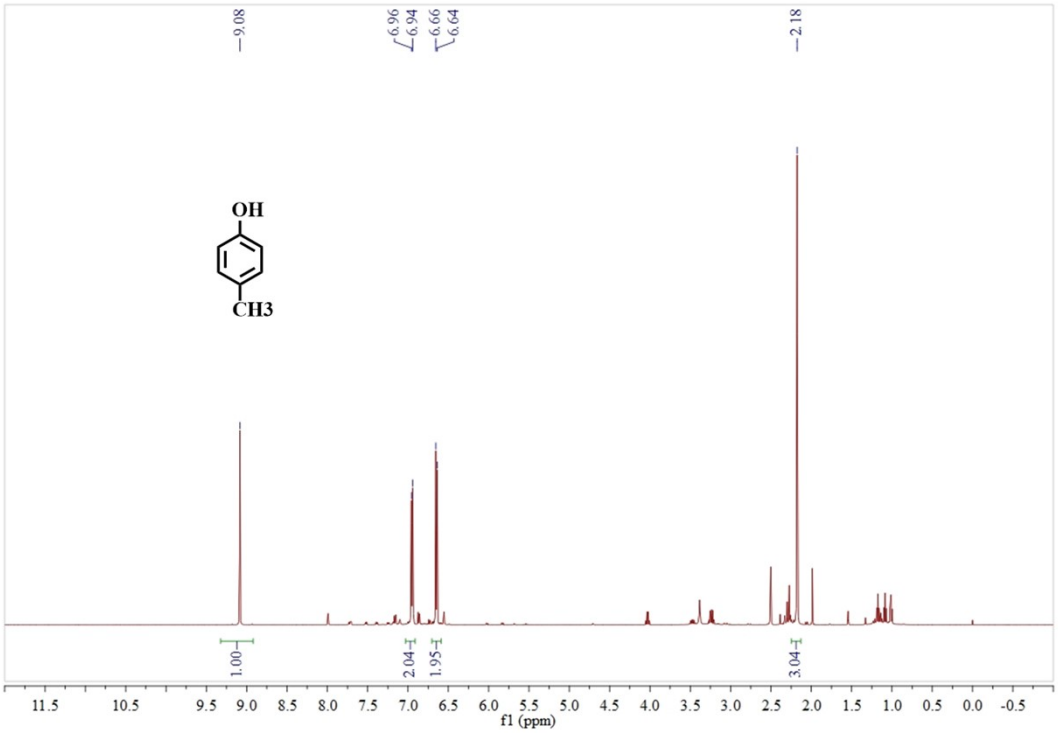

Figure S12. ^{1}H NMR spectrum of p-Cresol

^{1}H NMR (500 MHz, DMSO) δ 9.08 (s, 1H), 6.95 (d, J = 8.3 Hz, 2H), 6.65 (d, J = 8.4 Hz, 2H), 2.18 (s, 3H).

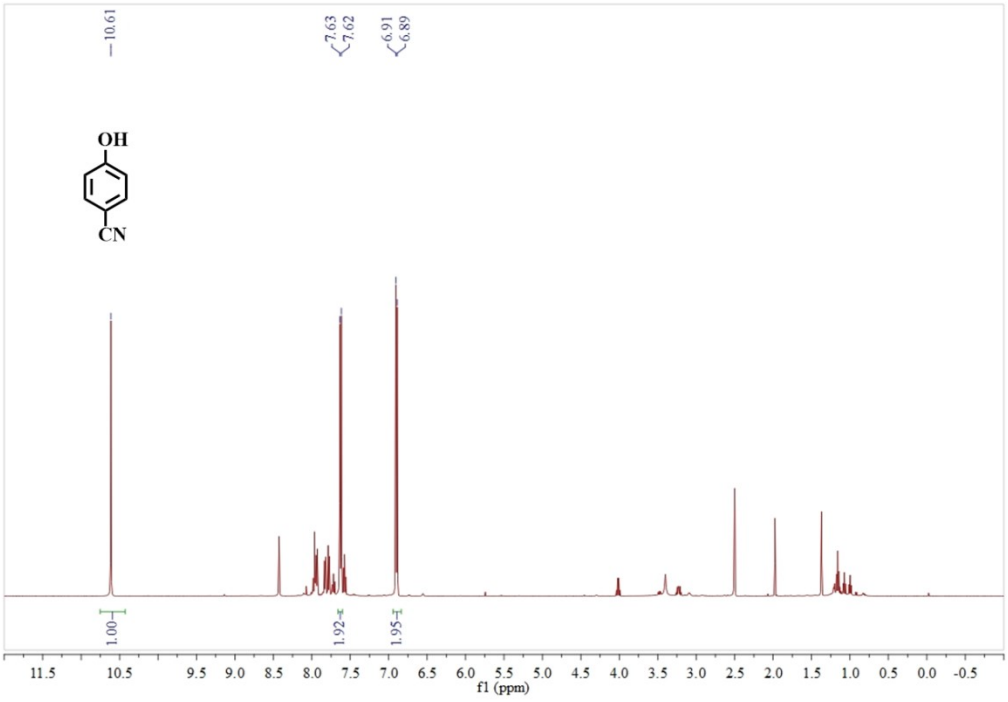

Figure S13. ^{1}H NMR spectrum of 4-Cyanophenol

^{1}H NMR (500 MHz, DMSO) δ 10.61 (s, 1H), 7.63 (d, J = 8.7 Hz, 2H), 6.90 (d, J = 8.8 Hz, 2H).

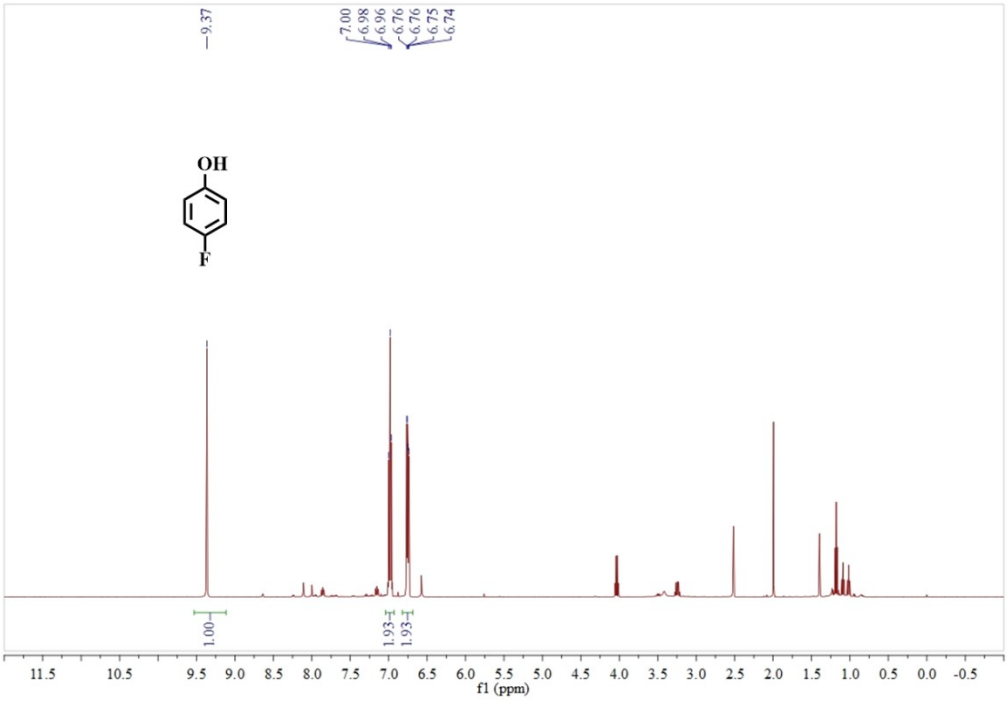

Figure S14. ^{1}H NMR spectrum of 4-Fluorophenol

^{1}H NMR (500 MHz, DMSO) δ 9.37 (s, 1H), 6.98 (t, J = 8.9 Hz, 2H), 6.75 (dd, J = 9.0, 4.5 Hz, 2H).

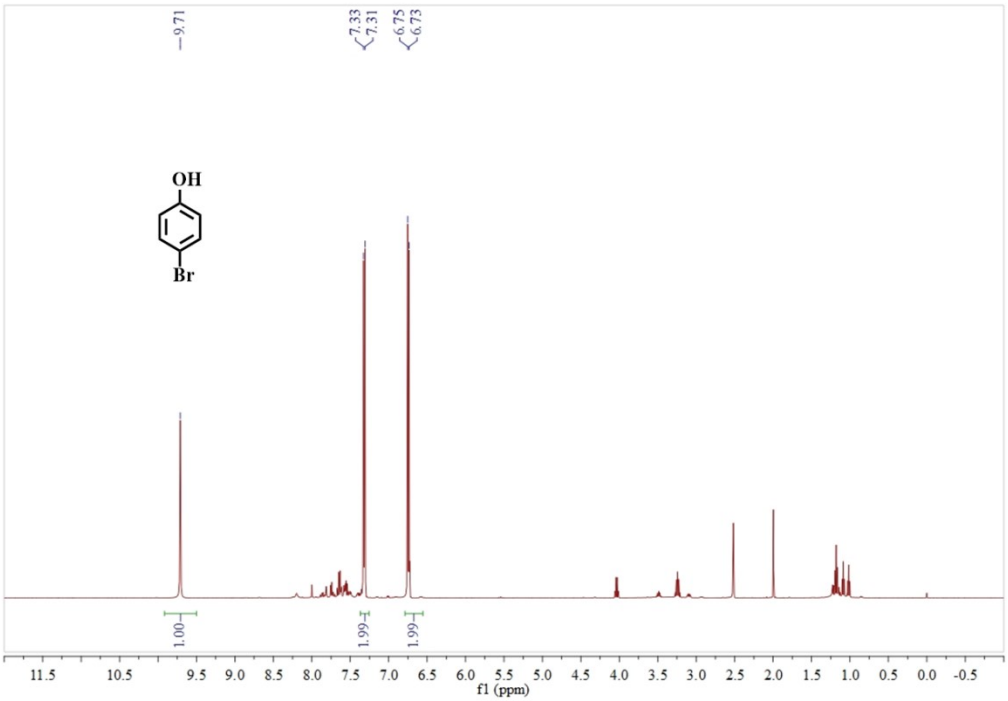

Figure S15. ^{1}H NMR spectrum of 4-Bromophenol

^{1}H NMR (500 MHz, DMSO) δ 9.71 (s, 1H), 7.32 (d, J = 8.8 Hz, 2H), 6.74 (d, J = 8.9 Hz, 2H).

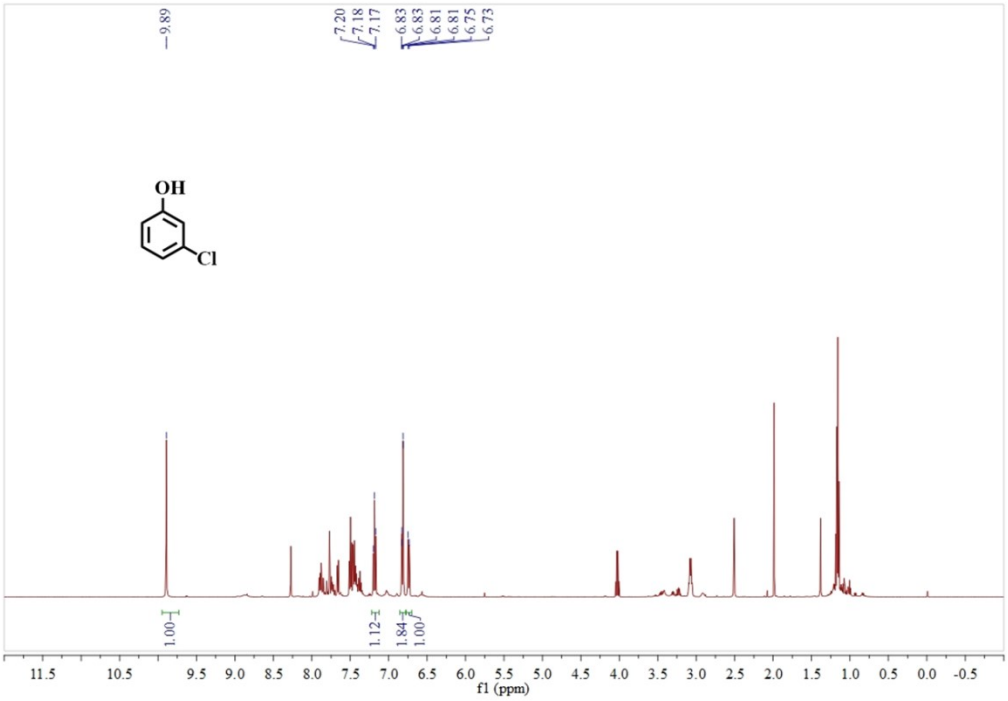

Figure S16. ^{1}H NMR spectrum of 3-Chlorophenol

^{1}H NMR (500 MHz, DMSO) δ 9.89 (s, 1H), 7.18 (t, J = 8.1 Hz, 1H), 6.82 (dd, J = 8.3, 1.6 Hz, 2H), 6.74 (d, J = 9.4 Hz, 1H).

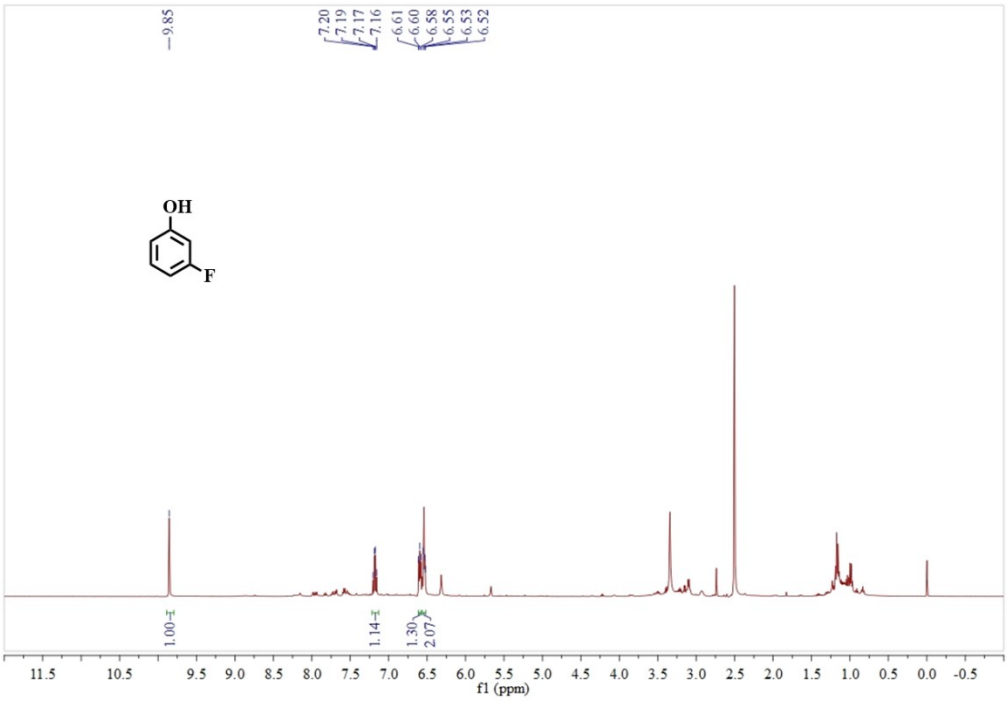

Figure S17. ^{1}H NMR spectrum of 3-Fluorophenol

^{1}H NMR (500 MHz, DMSO) δ 9.85 (s, 1H), 7.18 (dd, J = 15.6, 8.0 Hz, 1H), 6.60 (s, 1H), 6.56 – 6.52 (m, 2H).

5. Supplementary References

S1 B. Godin, J. Vaissermann, P. Herson, L. Ruhlmann, M. Verdaguer, P. Gouzerh, Coordination chemistry of the hexavacant tungstophosphate $[H_2P_2W_{12}O_{48}]^{12-}$: synthesis and characterization of iron(III) complexes derived from the unprecedented $\{P_2W_{14}O_{54}\}$ fragment, *Chem. Commun.*, 2005, 5624.

S2 Dolomanov, O.V., Bourhis, L.J., Gildea, R.J, Howard, J.A.K. & Puschmann, OLEX2: a complete structure solution, refinement and analysis program, H. (2009), *J. Appl. Cryst*. 42, 339-341.

S3 Bourhis, L.J., Dolomanov, O.V., Gildea, R.J., Howard, J.A.K., Puschmann, The anatomy of a comprehensive constrained, restrained refinement program for the modern computing environment – Olex2 dissected, H. (2015). *Acta Cryst*. A71, 59-75.

S4 Sheldrick, G.M. (2015). SHELXT-Integrated space-group and crystal-structure determination, *Acta Cryst*. C71, 3-8.

S4 P. F. Wei, M. Z. Qi, Z. P. Wang, S. Y. Ding, W. Yu, Q. Liu, L. K. Wang, H. Z. Wang, W. K. An, W. Wang, Benzoxazole-Linked Ultrastable Covalent Organic Frameworks for Photocatalysis, *J. Am. Chem. Soc.,* 2018, 140, 4623–4631.

S5 Martin, C. R.; Park, K. C.; Leith, G. A.; Yu, J.; Mathur, A.; Wilson, G. R.; Gange, G. B.; Barth, E. L.; Ly, R. T.; Manley, O. M.; Forrester, K. L.; Karakalos, S. G.; Smith, M. D.; Makris, T. M.; Vannucci, A. K.; Peryshkov, D. V.; Shustova, N. B. Stimuli-Modulated Metal Oxidation States in Photochromic MOFs. *J. Am. Chem. Soc.,* 2022, ***144***, 4457–4468.

S5 Y. Xiao, C. M. Zhu, R. B. Liang, Y. L. Huang, C. H. Hai, J. R. Chen, M. Li, J. J. Zhong, X. C. Huang, Building a cobaloxime-based metal–organic framework for photocatalytic aerobic oxidation of arylboronic acids to phenols, *Chem. Commun.* 2023, **59**, 2239–2242.

S6 W. Ren, J. Cheng, H. Ou, C. Huang, M. Anpo, X. Wang, Optimizing the crystallization process of conjugated polymer photocatalysts to promote electron transfer and molecular oxygen activation, *J. Catal*., 2020, **389**, 636–645.

S7 X. Dong, H. Hao, F. Zhang, X. Lang, Blue light photocatalysis of carbazole-based conjugated microporous polymers: Aerobic hydroxylation of phenylboronic acids to phenols, *Applied Catalysis B: Environmental.,* 2022, **309**, 121210.

S8 X. Yu, S.M. Cohen, Photocatalytic metal–organic frameworks for the aerobic oxidation of arylboronic acids, *Chem. Commun.,* 2015, **51**, 9880–9883.

S9 L. Sun, R. Li, W. Zhan, F. Wang, Y. Zhuang, X. Wang, X. Han, Rationally Designed Double-Shell Dodecahedral Microreactors with Efficient Photoelectron Transfer: N-Doped-C-Encapsulated Ultrafine In_2O_3 Nanoparticles, Chem. Eur. J. 25 (2019) 3053–3060.

S10 J. Luo, X. Zhang, J. Zhang, Carbazolic Porous Organic Framework as an Efficient, Metal-Free Visible-Light Photocatalyst for Organic Synthesis, ACS Catal. 5 (2015) 2250–2254.

S11 H. P. Liang, Q. Chen, B. H. Han, Cationic Polycarbazole Networks as Visible-Light Heterogeneous Photocatalysts for Oxidative Organic Transformations, ACS Catal. 8 (2018) 5313–5322.